Supplementary Information

Redox Flow Batteries: How To Determine Electrochemical Kinetic Parameters

Hao Wang,[†,‡,⊥] Sayed Youssef Sayed,[†,‡,⊥,*] Erik J. Luber,[†,‡] Brian C. Olsen,[†,‡] Shubham M. Shirurkar,[§] Sankaranarayanan Venkatakrishnan,[§] Ushula M. Tefashe,[†] Anna K. Farquhar,[†] Eugene S. Smotkin,[§] Richard L. McCreery,[†] and Jillian M. Buriak[†,‡,*]

[†]Department of Chemistry, University of Alberta, 11227 Saskatchewan Drive, Edmonton, Alberta T6G 2G2, Canada.

[‡]Nanotechnology Research Center, National Research Council Canada, 11421 Saskatchewan Drive, Edmonton, Alberta T6G 2M9, Canada.

[§]Department of Chemistry and Chemical Biology, Northeastern University, Boston, Massachusetts 02115, United States

[⊥]These authors contributed equally to this work.

* E-mail: (S.Y.S) synagy@ualberta.ca, (J.M.B) jburiak@ualberta.ca,

Contents

1. Additional information regarding reversible, irreversible, and quasireversible redox systems

1.1 Reversible redox systems Reversible electrochemical reactions are characterized by high rates of charge transfer (high standard rate constants, *e.g.*, $k^0 > 10^{-1}$ cm s^{-1}).[S1] The measured current is dictated by the slowest process - the diffusional mass transport of redox species. The charge transfer for a reversible redox reaction (Ox + e^- ⇋ Red) occurs instantly at the electrode surface, and a dynamic equilibrium is established that corresponds to the Nernst relationship: electrode potential $E = E^{0\prime} + (RT/nF)\ln(O_{\text{surf.}}/R_{\text{surf.}})$.[S2] Thus, the surface concentrations are only a function of the electrode potential and are not influenced by the rate of charge transfer. Further, the shape of the characteristic voltammograms is correlated to the potential-dependent changes in the surface concentrations, as well as the accompanied diffusional mass transport. In a typical reductive CV scan for a reversible redox reaction (Figure S1), the scan starts at an electrode potential more positive than that for $E^{0\prime}$, and only a non-faradaic (capacitive) current, i_C, passes. As the potential scan approaches $E^{0\prime}$, reduction begins and a faradaic current starts to pass. This step should result in a decrease in the concentration of the

oxidized species at the vicinity of the electrode surface, creating a diffusion layer. The increase in current with the continuous scan toward more negative potentials is attributed to the increasing flux to the surface across the diffusion layer.[S3] At potentials more negative than $E^{0'}$, the surface concentration of the oxidized species decreases and nearly approaches zero, resulting in maximum flux (current). At more negative potentials, the current then decays with a complete depletion of the oxidized species on the electrode surface.[S2,S3] These processes result in a peaked current-potential curve, Figure S1. Similar current-potential features are typically observed for a reverse scan. The peak current is related to the scan rate according to the Randles–Sevcik equation,

$$i_p = 2.69 \times 10^5 n^{3/2} A C^* D^{1/2} v^{1/2} \qquad (S1)$$

at 25 °C where C^* is the bulk concentration. The diffusion coefficient, D, can be extracted from the slope of a linear plot of the peak current versus the square root of the scan rate. Other criteria that describe reversible voltammograms are listed below:

(1) k^0 >>> mass transfer coefficient;

(2) peak potential (E_p) is independent of the scan rate, Figure 2 in the main text;

(3) peak separation ΔE_p = 57/n mV;

(4) anodic peak current (i_{pa}) and cathodic peak current (i_{pc}) meet: i_{pa}/i_{pc} = 1.

1.2 Irreversible Redox Systems An irreversible electrochemical process is typically limited by sluggish charge transfer kinetics (*e.g.*, k^0 < 10^{-5} cm s^{-1}), as represented by the green plot in Figure 2.[S1] High overpotentials are required to drive charge transfer between the electrode surface and electroactive species, and thus large peak separations are usually observed, compared to those for reversible and quasireversible systems. No equilibrium is established and, thus, the Nernst equation does not apply. The measured current is limited by the rate of the charge transfer, where the peak current is related to the rate constant according to

$$\begin{aligned} i_p &= 0.227 F A C^* k^0 \exp\left(\frac{-\alpha F (E_p - E^{0'})}{RT}\right) \\ \Rightarrow \ln(i_p) &= \ln(0.227 F A k^0 C^*) - (\alpha F/RT)(E_p - E^{0'}) \end{aligned} \qquad (S2)$$

Provided that $E^{0'}$ is known, a linear plot of $\ln(i_p)$ *vs* $(E_p - E^{0'})$ at different scan rates should give a slope of $-\alpha F/RT$ and an intercept that is a function of the rate constant k^0. Other characteristics of irreversible redox systems are listed below:

(1) k^0 <<< mass transfer coefficient;

(2) $i_p = 2.99 \times 10^5 n^{3/2} \alpha^{1/2} A C^* D^{1/2} v^{1/2}$;

(3) E_p shifts to higher potential as the scan rate increases;

(4) $|E_p - E_{p/2}| = (48/\alpha n)$ mV at 25 °C.

1.3 Quasireversible Redox Systems A quasireversible redox system falls into an intermediate regime between reversible and irreversible systems, as shown in Figure 2 in the main text; in this regime, k^0 falls between 10^{-1} and 10^{-5}.[S1] The current is limited by both the charge transfer kinetics and mass transport. Whichever of the two is the smallest (the rate-determining step) controls the reversibility of the redox reaction. The scan rate contributes significantly to the shape of cyclic voltammograms for quasireversible systems by altering the mass transfer coefficient $m_t = (DFv/RT)^{1/2}$.[S4] Matsuda and Ayabe[S5] proposed a dimensionless parameter (Λ), $\Lambda = k^0/(DFv/RT)^{1/2}$, to determine the apparent reversibility of redox species according to the following kinetic zones:

Reversibility: $\Lambda > 15$

Quasireversible: $15 \geq \Lambda \geq 10^{-2(1+\alpha)}$

Irreversible: $\Lambda < 10^{-2(1+\alpha)}$

At a low scan rate, the shape of the CV approaches the reversible case as the ratio of k^0/m_t increases. At high scan rates, however, the k^0/m_t ratio decreases and the CV resembles that of the voltammogram of an irreversible redox reaction. We have noted a misunderstanding in the literature regarding the relationship between peak current and the square root of the scan rate for quasireversible systems. Please note that in contrast to reversible and irreversible systems, i_p for quasireversible systems is not proportional to $v^{1/2}$, due to the transition from reversible to irreversible voltammograms with scan rate.[S6] Other criteria that describe quasireversible systems include:

(1) E_p depends on the scan rate;

(2) ΔE_p increases with the scan rate.[S2]

2. Key experimental points for cyclic voltammograms

First, precleaning of the working electrodes is highly essential to remove any contaminants on the surface that might mislead the measurements of the kinetic parameters; we refer the reader to a useful tutorial by Dempsey and co-workers.[S7] A precleaning protocol usually starts with mechanical polishing of the electrode surface in a water-alumina slurry followed by rinsing and sonicating in ultrapure water.[S7–S9] Electrochemical cycling, until a steady-state is reached, can also be used subsequently to further remove different kinds of surface contaminants.[S8,S10]

Second, the peak current can be used to determine various kinetic parameters for redox species in concern. For accurate determination of the faradaic peak current, a correction has to be performed to cancel out the background current, resulting from (1) charging the electrode double layer (capacitive current), and (2) redox reactions of adventitious species in the solvent or on the electrode surface (residual current). The capacitive current varies linearly with the scan rate ($i_C = AC_d v$, where i_C, A, C_d, and v are the capacitive current, electrode area, double-layer capacitance, and scan rate, respectively).[S2] Hence, a significant contribution from the capacitive current can be encountered at high scan rates.[S3,S9] To rule out the capacitive current, the actual value of the peak current should be measured from the baseline current at the initial stages of the voltammogram, Figure S1. Alternatively, at the same peak potential, the peak current can be determined by subtracting the background current of a separate cyclic voltammogram run at the same scan rate in the absence of the redox species.

Third, while running cyclic voltammograms, the potentiostat controls the potential on the working electrode with respect to the reference electrode. However, the controlled potential ($E_{\text{controlled}}$) is the sum of the actual potential (E_{actual}) on the electrode surface and the ohmic potential (iR_u); $E_{\text{controlled}} = E_{\text{actual}} + iR_u$. The ohmic resistance, or uncompensated resistance (R_U), results from the resistance of the electrolyte as well as

contact resistances. R_U can be determined by electrochemical impedance spectroscopy (EIS).[S9] The iR_u drop is a function of the measured faradic current, which increases with $v^{1/2}$. Thus, increasing the scan rate results in increasing the ohmic drop and shifting the peak potential to higher values, inducing false peak separation (ΔE_p) between anodic and cathodic peaks. For accurate determination of ΔE_p, it is highly recommended to correct the cyclic voltammograms for the potential drop resulting from the ohmic resistance.[S9,S11,S12]

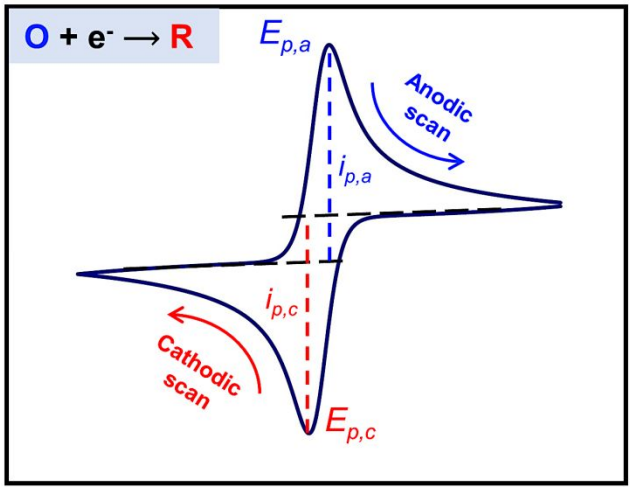

Figure S1. A simulated cyclic voltammogram for a reversible system showing the exact determination of peak current from the baseline. This plot is expected with low background current (without redox species present), or after subtraction of the background current.

3. Steps for constructing Koutecký-Levich plots

Equation used for simulating RDE plots in Figure 6 in the main text:

$$i = (1 - \frac{i}{i_{l,c}})i_0\exp(\frac{-\alpha F(E - E_{eq})}{RT}) - (1 - \frac{i}{i_{l,a}})i_0\exp(\frac{(1-\alpha)F(E - E_{eq})}{RT})$$
$$i_{l,c} = 0.62nFAD_O^{2/3}\nu^{-1/6}C_O^*\,\omega^{1/2} \qquad (S3)$$
$$i_{l,a} = 0.62nFAD_R^{2/3}\nu^{-1/6}C_R^*\,\omega^{1/2}$$

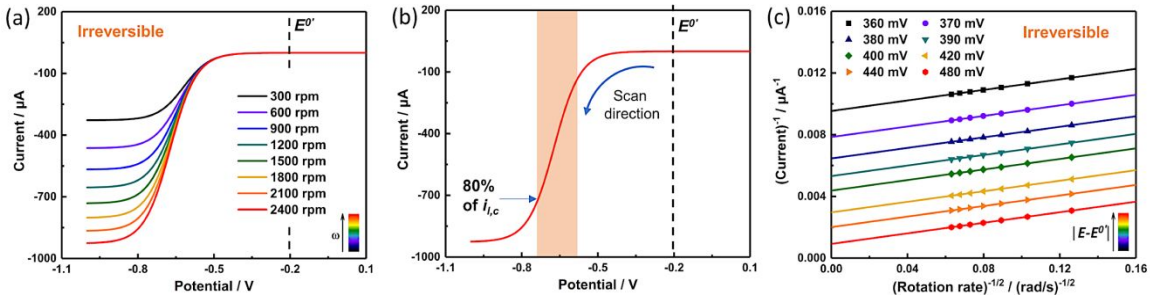

Figure S2. (a) RDE voltammograms for an irreversible system with k^0 = 10^{-6} cm²/s at different rotation rates. (b) RDE voltammogram at 2400 rpm, showing the selected current region (< 80% of the limited current) for mass transfer correction for the measured current. (c) Koutecký-Levich plots for an irreversible system at different rotation rates.

Table S1. Simulated parameters for irreversible and quasireversible systems in Figures 6a and 6d.

Parameter	Value
α	0.5
C_O^* (mol cm^{-3})	5×10^{-6}
C_R^* (mol cm^{-3})	10^{-13}
D_O & D_R (cm^2/s)	10^{-5}
Electrode area A (cm^2)	0.19625
Kinematic viscosity (cm^2 /s)	0.01024
$E^{0'}$ (V)	-0.2
Irreversible rate constant k^0 (cm s^{-1})	1×10^{-6}
Quasireversible rate constant k^0 (cm s^{-1})	0.003

Table S2. Inverse currents $1/i$ for Angular velocities, ω (rpm) and Potentials (V) as indicated used to construct the Koutecký-Levich plot for an irreversible system in Figure 6b.

Potential (V)	300 rpm	600 rpm	900 rpm	1200 rpm	1500 rpm	1800 rpm	2100 rpm	2400 rpm
-0.56	-0.0125	-0.0116	-0.0112	-0.0110	-0.0110	-0.0107	-0.0106	-0.0106
-0.57	-0.0109	-0.0100	-0.0096	-0.0093	-0.0092	-0.0090	-0.0090	-0.0089
-0.58	-0.0095	-0.0086	-0.0082	-0.0079	-0.0078	-0.0077	-0.0076	-0.0075
-0.59	-0.0083	-0.0074	-0.0071	-0.0068	-0.0066	-0.0065	-0.0064	-0.0063
-0.6	-0.0074	-0.0065	-0.0061	-0.0059	-0.0057	-0.0057	-0.0055	-0.0054
-0.62	-0.0060	-0.0051	-0.0047	-0.0044	-0.0043	-0.0042	-0.0041	-0.0040
-0.64	-0.0050	-0.0041	-0.0038	-0.0035	-0.0033	-0.0032	-0.0031	-0.0030
-0.68	-0.0039	-0.0030	-0.0027	-0.0024	-0.0022	-0.0021	-0.0020	-0.0020

We refer the reader to the publications by Shao-Horn and co-workers[S9,S13] recommending mass transfer correction for current data below 80% of the diffusion limited current to minimize errors in the Koutecký-Levich analysis (see Figure S2).

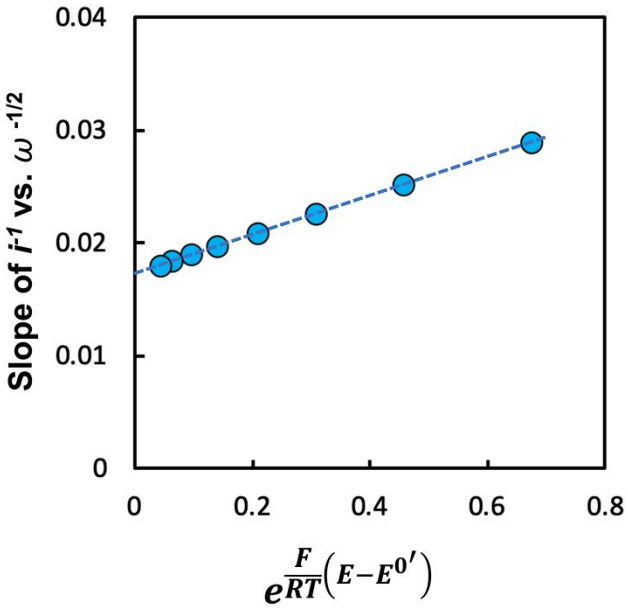

Figure S3. Plot the slope of the i^{-1} vs. $\omega^{-1/2}$ plots for quasireversible system (Figure 6e) vs. $e^{\frac{F}{RT}(E-E^{0\prime})}$.

The intercept is a function of the diffusion coefficient of the oxidized species, D_O, and a slope that is a function of diffusion coefficient of D_R of the newly formed reduced species, R.

4. Determination of the standard rate constant (k^0) using sampled current voltammetry (SCV)

In this section, we describe a supplementary technique that would act as a double-check to support the kinetic values obtained in sections 1 and 2, in the main text of the manuscript. SCV is a potential-relaxation technique that results in sigmoidal current-voltage plots for the three kinetic regimes, reversible, quasireversible and irreversible. Examples of accessible parameters from the wave height (i_d) are the number of electrons (n), diffusion coefficient (D), bulk concentration, and electrode area (A). For quasireversible and irreversible systems, SCV can also provide information on kinetic parameters such as k^0 and α, *vide infra*. In SCV, a series of step potentials, from the rest

potential ($E_{\text{appl.}} < E^{0'}$) to the desired potential ($E_{\text{appl.}} > E^{0'}$), should be applied. For each of the selected step potentials, the current should decay with time and recorded at a fixed decay time ($t = \tau$), Figure S4. A sigmoidal current-potential plot is thus obtained. At high potentials ($E_{\text{appl.}} > E^{0'}$), rapid depletion of the analyte at the electrode surface occurs and the process would be controlled by only the diffusion of the analyte to the electrode and thus the solution has to be unstirred. In this case, the measured current is the diffusion-limited current (i_d) and Cottrel Equation S4 applies.

$$i_d = \frac{nFAD^{1/2}C^*}{\pi^{1/2}t^{1/2}} \qquad (S4)$$

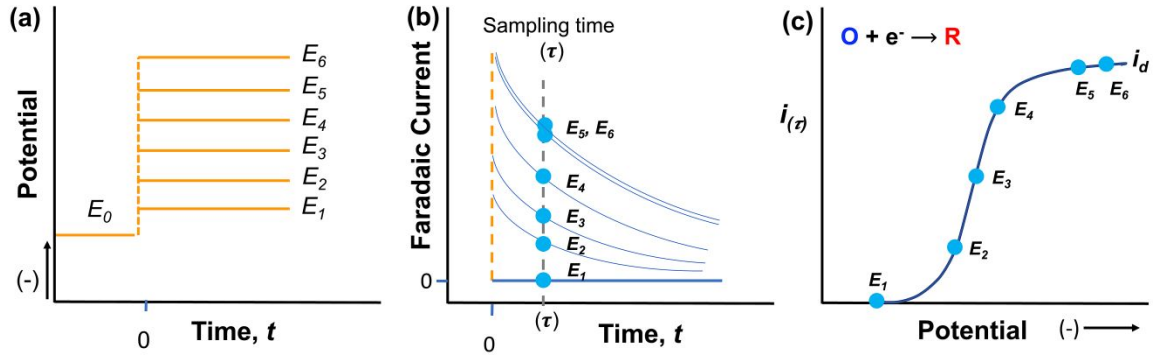

Figure S4. Sampled current voltammetry procedures. (a) Potential step experiments at different increasing reducing potentials. (b) Current-time decay for each of the applied potential steps and illustrates the sampling time (same for all potential steps). (c) Sampled current voltammogram.

For solutions in which only one single species exists (either oxidized or reduced species, O or R, respectively), Equation S5 represents the dependence of the current, in SCV, on the applied potential and time for reversible, quasireversible, and irreversible systems, Figure S5. Please note that the function $F_1(\lambda)$ approaches unity for reversible systems and thus resulting in Equation S6. For irreversible systems, however, $K_b/K_f = \Theta = 0$, thus Equation S5 is simplified to Equation S7.

$$
\begin{aligned}
i &= \frac{i_d}{(1+\xi\theta)}F_1(\lambda) \\
\text{Where } \xi &= \left(\frac{D_O}{D_R}\right)^{1/2};\ \ \theta = \exp\left(\frac{nF(E-E^{0'})}{RT}\right); \\
F_1(\lambda) &= \pi^{1/2}\lambda\exp(\lambda^2)\mathrm{erfc}(\lambda); \\
\lambda &= Ht^{1/2} = \frac{k_f t^{1/2}}{D_O^{1/2}}(1+\xi\theta); \\
k_f &= k_0\exp\left(\frac{-\alpha F(E-E^{0'})}{RT}\right)
\end{aligned}
\qquad (S5)
$$

For a reversible system:

$$i = \frac{i_d}{(1+\xi\theta)} \qquad (S6).$$

For an irreversible system:

$$\frac{i}{i_d} = F_1(\lambda) = \pi^{1/2}\lambda\exp(\lambda^2)\mathrm{erfc}(\lambda) \qquad (S7),$$

where λ for irreversible systems equals $k_f t_{1/2}/D^{1/2}$.

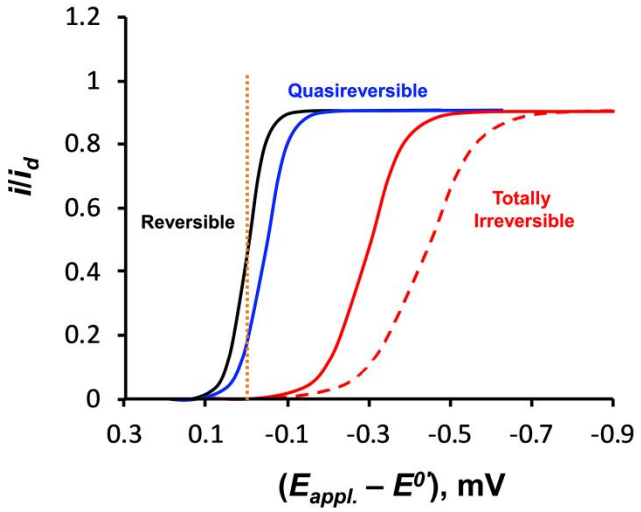

Figure S5. Examples of sampled current voltammetry for the three different kinetics regime.

For quasireversible systems, the kinetics parameters (k^0 and α) can be determined by fitting the experimental plot of i/i_d vs. $(E_{\text{appl.}} - E^{0'})$ to the theoretical function in Equation S5. The fitting can be done by employing a nonlinear least-squares fitting algorithm such as Levenberg-Marquardt. For an example of curve fitting for SCV, we refer the reader to published work by Friedl *et al.*[S14]

In potential step experiments, the charging (non-faradaic) current contributes to the faradaic current during a period of about five times the cell time constant (R_uC_d, where R_u is the uncompensated resistance and C_d is the double layer capacitance).[S2] Thus, the sampling time has to be larger than R_uC_d. Using ultramicroelectrodes (UME) one can minimize the cell time constant (R_uC_d) . Fitting and analysis of the steady-state voltammograms observed using UME for quasireversible systems can be done by with Equation S8. The second method for extracting the kinetic parameters for quasireversible systems involves comparing the differences ($E_{1/4} - E_{1/2}$) and ($E_{3/4} - E_{1/4}$) from the steady-state voltammograms observed using UME to the tables published by Mirkin and Bard for these differences and the correspondings sets of k^0 and α, where $E_{1/4}$, $E_{1/2}$, and $E_{3/4}$ are the potentials at i = 1/4, 1/2, and 3/4 i_d, respectively.[S15]

$$i = \frac{FAD_OC_O^*}{r_0}\left[\frac{\kappa}{1+\kappa(1+\xi^2\theta)}\right] \qquad (S8),$$

where r_0 is the radius of the UME and $\kappa = r_0k_f/D$.

For irreversible systems, similar to quasireversible systems, fitting SCV or the steady-state voltammograms using Equation S7 and Equation S9, respectively, can allow for the determination of k^0 and α. There are two other alternative methods for determining k^0 and α for irreversible systems. The first method involves calculating α from the slope of E vs. $\log(i_d - i)/i$ for the steady-state voltammograms according to Equation S10. The intercept at $E^{0'}$ can provide the k^0 value provided that (r_0/D) is known. The second method is based on Tomes' criterion, as shown in Table S3, the difference ($E_{3/4} - E_{1/4}$) for totally irreversible systems can provide α directly, where ($E_{3/4} - E_{1/4}) = 45.0/\alpha$ and $59.1/\alpha$ for linear diffusion at planar electrodes and steady-state voltammograms at UME, respectively. Once α is determined, k^0 can be calculated from Equation S11 from the half-wave potential ($E_{1/2}$) provided that $E^{0'}$ is known. For reversible systems, the number of electrons can be extracted either from the slope of the sigmoidal wave or from the Tomes' criterion as shown in Table S3.

$$\frac{i}{i_d} = \frac{\kappa}{1+\kappa} \qquad (S9)$$

by substituting for κ and $k_f = k^0 \exp(-\alpha F/RT)(E - E^{0'})$, one obtains the potential-current Equation S9

$$E = E^{0'} + \frac{RT}{\alpha F}\ln\left(\frac{r_0 k^0}{D}\right) + \frac{RT}{\alpha F}\ln\left(\frac{i_d - i}{i}\right) \qquad (S10),$$

where half-wave potential,

$$E_{1/2} = E^{0'} + \frac{RT}{\alpha F}\ln\left(\frac{r_0 k^0}{D}\right) \qquad (S11).$$

Table S3. Characteristics for the current-potential wave observed in sampled current voltammetry plots of E vs. $\log(i_d - i)/i$ at 25 °C. *Using ultramicroelectrodes (UME), electrodes of radii less than 25 μm.[2] This table was adapted from the textbook of A. J. Bard.[S2]

Kinetic Regime	Linear diffusion at planar electrodes		Steady-state*	
	Slope (mV)	$E_{3/4} - E_{1/4}$ (mV)	Slope (mV)	$E_{3/4} - E_{1/4}$ (mV)
Reversible ($n \geq 1$)	Linear, $59.1/n$	$56.4/n$	Linear, $59.1/n$	$56.4/n$
Quasireversible ($n = 1$)	Slightly nonlinear	Between 56.4 and $45.0/\alpha$	Nonlinear	Between 56.4 and 56.4/α
Irreversible ($n = 1$)	Slightly nonlinear	45.0/α	Linear, 59.1/α	56.4/α

5. Criteria for constructing Tafel plots

The Tafel equation, which relates the rate of an electrochemical reaction to the applied overpotential (Equation S12), has been used for decades to determine electrochemical kinetic parameters for redox reactions. In the high overpotential linear region in a Tafel plot (Figure S6), the slope and intercept are function of α and k^0, respectively. Moreover, this linear region of the Tafel plot represents a contribution of less than 1% of the backward reaction, which is verified at η > 118 mV at 25 °C. At low η (< 118 mV), the reverse reaction cannot be neglected and as a result, the plot deviates from linearity. It has been brought to our attention that the representation of the Tafel plots in a few of the recent papers on RFBs is based on stationary (unstirred) cyclic voltammograms. We would like to emphasize that the Tafel equation is derived from the Butler-Volmer equation under the condition of no mass transfer, *i.e,* the surface concentration is almost equal to the bulk concentration. This condition requires well-stirred solutions and correction for any mass-transport effect.

$$\eta = \frac{RT}{\alpha F}\ln(i_0) - \frac{RT}{\alpha F}\ln(i) \qquad (S12)$$

$$i_0 = nFAk^0C \text{ (when } C_O^* = C_R^*) \qquad (S13)$$

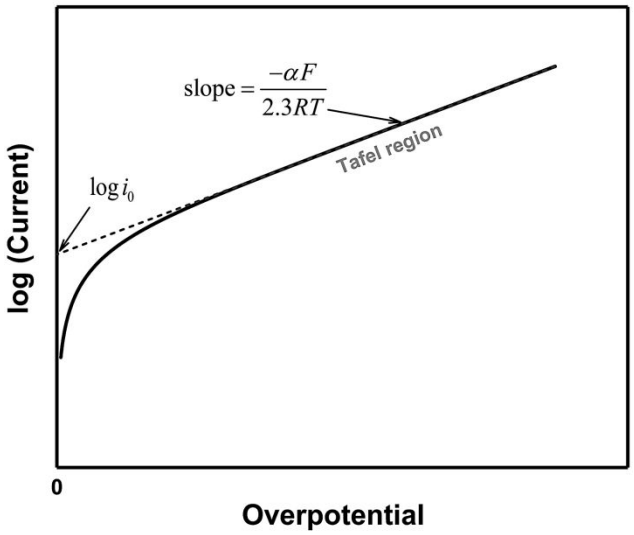

Figure S6. A Tafel plot for a cathodic branch of the current-potential curves for a one-step, one-electron, O + e^- ⇋ R reaction.

6. REFERENCES

S1. Heinze, J. Cyclic Voltammetry—"Electrochemical Spectroscopy". New Analytical Methods (25). *Angew. Chem. Int. Ed.* **1984**, *23*, 831–847.

S2. Bard, A. J. *Electrochemical Methods: Fundamentals and Applications*, 2nd ed.; Wiley, New York: 2001.

S3. Diamond, P. S. *Laboratory Techniques in Chemistry and Biochemistry*; Butterworths, London, 1966.

S4. Brownson, D. A. C.; Banks, C. E. *Interpreting Electrochemistry. In the Handbook of Graphene Electrochemistry*; Brownson, D. A. C., Banks, C. E., Eds.; Springer London: London, 2014; pp 23–77.

S5. Matsuda, H.; Ayabe, Y. Z. Theorie der Randles-Sevčikschen Kathodenstrahl-Polarographie. *Z. Electrochem.* **1955**, *59*, 494–503.

S6. Ozkan, S. A.; Kauffmann, J.-M.; Zuman, P. *Electroanalysis in Biomedical and Pharmaceutical Sciences*; Monographs in Electrochemistry; Springer Berlin Heidelberg: Berlin, Heidelberg, 2015.

S7. Elgrishi, N.; Rountree, K. J.; McCarthy, B. D.; Rountree, E. S.; Eisenhart, T. T.; Dempsey, J. L. A Practical Beginner's Guide to Cyclic Voltammetry. *J. Chem. Educ.* **2018**, *95*, 197–206.

S8. Sawant, T. V.; McKone, J. R. Flow Battery Electroanalysis. 2. Influence of Surface Pretreatment on Fe(III/II) Redox Chemistry at Carbon Electrodes. *J. Phys. Chem. C* **2019**, *123*, 144–152.

S9. Wei, C.; Rao, R. R.; Peng, J.; Huang, B.; Stephens, I. E. L.; Risch, M.; Xu, Z. J.; Shao-Horn, Y. Recommended Practices and Benchmark Activity for Hydrogen and Oxygen Electrocatalysis in Water Splitting and Fuel Cells. *Adv. Mater.* **2019,** e1806296.

S10. Li, D.; Wang, C.; Tripkovic, D.; Sun, S.; Markovic, N. M.; Stamenkovic, V. R. Surfactant Removal for Colloidal Nanoparticles from Solution Synthesis: The Effect on Catalytic Performance. *ACS Catal.* **2012**, *2*, 1358–1362.

S11. Van der Vliet, D.; Strmcnik, D. S.; Wang, C.; Stamenkovic, V. R.; Markovic, N. M.; Koper, M. T. M. On the Importance of Correcting for the Uncompensated Ohmic Resistance in Model Experiments of the Oxygen Reduction Reaction. *J. Electroanal. Chem.* **2010**, *647*, 29–34.

S12. Izquierdo, J.; Kranz, C. Electrochemical Techniques for Investigating Redox Active Macromolecules. *Eur. Polym. J* **2016**, *83*, 428–449.

S13. Sheng, W.; Gasteiger, H. A.; Shao-Horn, Y. Hydrogen Oxidation and Evolution Reaction Kinetics on Platinum: Acid *vs* Alkaline Electrolytes. *J. Electrochem. Soc.* **2010**, *157*, B1529–B1536.

S14.Friedl, J.; Lebedeva, M. A.; Porfyrakis, K.; Stimming, U.; Chamberlain, T. W. All-Fullerene-Based Cells for Nonaqueous Redox Flow Batteries. *J. Am. Chem. Soc.* **2018**, *140*, 401–405.

S15. Mirkin, M. V.; Bard, A. J. Simple Analysis of Quasi-Reversible Steady-State Voltammograms. *Anal. Chem.* **1992**, *64*, 2293–2302.